MATERIALS SCIENCE

Thermally assisted nanotransfer printing with sub–20-nm resolution and 8-inch wafer scalability

Tae Wan Park[1,2]*, Myunghwan Byun[3]*, Hyunsung Jung[1], Gyu Rac Lee[4], Jae Hong Park[5,6], Hyun-Ik Jang[5,6], Jung Woo Lee[7], Se Hun Kwon[7], Seungbum Hong[4], Jong-Heun Lee[2], Yeon Sik Jung[4†], Kwang Ho Kim[7,8†], Woon Ik Park[9†]

Nanotransfer printing (nTP) has attracted considerable attention due to its good pattern resolution, process simplicity, and cost-effectiveness. However, the development of a large-area nTP process has been hampered by critical reliability issues related to the uniform replication and regular transfer printing of functional nanomaterials. Here, we present a very practical thermally assisted nanotransfer printing (T-nTP) process that can easily produce well-ordered nanostructures on an 8-inch wafer via the use of a heat-rolling press system that provides both uniform pressure and heat. We also demonstrate various complex pattern geometries, such as wave, square, nut, zigzag, and elliptical nanostructures, on diverse substrates via T-nTP. Furthermore, we demonstrate how to obtain a high-density crossbar metal-insulator-metal memristive array using a combined method of T-nTP and directed self-assembly. We expect that the state-of-the-art T-nTP process presented here combined with other emerging patterning techniques will be especially useful for the large-area nanofabrication of various devices.

INTRODUCTION

Nanopatterning refers to a process by which to fabricate well-defined nanostructures with functionalities applicable to many electronic devices, such as transistors (*1*, *2*), displays (*3*, *4*), solar cells (*5*, *6*), energy generators (*7*, *8*), nonvolatile memories (*9*–*11*), and optical devices (*12*). In particular, photolithography, one of the most representative nanopatterning methods, is widely used to fabricate electronic devices with complex circuits (*13*). However, because of its physical resolution limitation and high process cost, several alternative technologies, such as extreme ultraviolet lithography (*14*), directed self-assembly (DSA) (*15*–*18*), nanoimprint lithography (*19*, *20*), nanotransfer printing (nTP) (*21*–*23*), atomic force microscope (AFM) lithography (*24*), and dip-pen lithography (*25*, *26*), have been consistently developed during the past several decades to allow periodic nanostructures to be obtained effectively with high precision. Among these various nanopatterning techniques, nTP has recently received considerable attention because it can capably generate specific functional nanostructures with two-dimensional (2D) and 3D pattern geometries (*27*) at a low process cost. The nTP process has excellent patterning capabilities when used for pattern formation on a range of arbitrary substrates, including flexible surfaces (*28*–*30*), which cannot be patterned by conventional lithography methods.

For these reasons, many research groups focusing on patterning technologies have suggested various innovative nTP techniques to form a variety of nanoscale-to-microscale patterns for useful nanofabrication processes. For example, Rogers's group reported a fast and simple nTP process based on elastomeric stamps capable of generating complex 2D and 3D metallic and semiconducting structures on both planar and nonplanar substrates (*31*). Jeong's group suggested wet-responsive and biocompatible hydrogel adhesive films for efficient transfer printing of functional membranes (*32*). Because of the excellent adhesion capabilities of hydrogels, metallic and nonmetallic nanomembranes can be reliably transferred onto diverse surfaces, such as flexible or rigid substrates or even human skin. Recently, Xu and Lee's group presented an environmentally friendly transfer printing process that enables the physical delivery of 4-inch wafer-scale thin-film integrated circuits with functional nanomaterials through effectual separation from the fabrication wafer (*33*). These findings imply that, to extend the versatility of the nTP process for the useful fabrication of nanodevices, it is very important to develop a more practical and simpler patterning strategy that is compatible with the electronic device application processes on various substrates (*34*, *35*).

However, despite the excellent patternability of these useful nTP methods that allow the formation of well-defined nanopatterns, they still have critical challenges given their pattern resolution limit of approximately 50 nm, which is determined by the master mold. Also, the insufficient transfer yield caused by the use of elastomeric molds also prevents large-scale production. To overcome these limitations, we previously demonstrated a solvent-injected nTP (S-nTP) process capable of realizing the pattern generation of functional 2D and 3D structures in the sub–10-nm to micrometer size range. High-density nanostructures in the sub–10-nm regime are effectively obtained using an ultrafine nanotemplate prepared by the DSA of block copolymers (BCPs) as a master mold (*36*). Nevertheless, the S-nTP process is linked to fundamentally critical issues in terms of large-area scalability. During the S-TP process, solvent vapor injection is difficult to control uniformly over a large area. It is therefore challenging to produce well-defined patterns at a wafer scale, which is imposed by long-range registration and defectivity

[1]Electronic Convergence Materials Division, Korea Institute of Ceramic Engineering & Technology (KICET) 101 Soho-ro, Jinju 52851, Republic of Korea. [2]Department of Materials Science and Engineering, Korea University, Seoul 02841, Republic of Korea. [3]Department of Advanced Materials Engineering, Keimyung University, 1095 Dalgubeol-daero, Daegu 42601, Republic of Korea. [4]Department of Materials Science and Engineering, Korea Advanced Institute of Science and Technology (KAIST), 291 Daehak-ro, Yuseong-gu, Daejeon 34141, Republic of Korea. [5]Division of Nano-Convergence Technology, Korea National NanoFab Center (NNFC), 291 Daehak-ro, Daejeon 34141, Republic of Korea. [6]NanoIn-Inc, 291 Daehak-ro, Korea National NanoFab Center (NNFC), Daejeon 34141, Republic of Korea. [7]School of Materials Science and Engineering, Pusan National University (PNU), Busandaehak-ro 63beon-gil, Geumjeong-gu, Busan 46241, Republic of Korea. [8]Global Frontier R&D Center for Hybrid Interface Materials (HIM), Busandaehak-ro 63beon-gil, Geumjeong-gu, Busan 46241, Republic of Korea. [9]Department of Materials Science and Engineering, Pukyoung National University (PKNU), 45 Yongso-ro, Nam-gu, Busan 48513, Republic of Korea.
*These authors contributed equally to this work.
†Corresponding author. Email: ysjung@kaist.ac.kr (Y.S.J); kwhokim@pusan.ac.kr (K.H.K); thane0428@pknu.ac.kr (W.I.P)

issues. Accordingly, a solvent-free transfer principle capable of nanopatterning at a wafer scale should be developed for successful implementation in large-area device applications.

Here, we introduce a very useful thermally assisted nTP (T-nTP) technique that can be used to create various periodic nanostructures on the 8-inch wafer using a heat-rolling press system that offers uniform pressure and heat. After the replication of well-ordered nanopatterns from an 8-inch Si master wafer, the functional nanostructures on a polymeric replica pattern can be transfer-printed onto the desired substrates after weakening the adhesion between the adhesive film and the replica pattern through a uniform heat-injection process. We also demonstrate reliable pattern formation of diverse morphological geometries consisting of various metallic and semiconducting materials with functionalities on diverse substrates via solvent-free T-nTP. In addition, we demonstrate how to obtain ultrahigh-resolution patterns of sub–20-nm lines and hierarchical 3D stacked nanostructures by using a combined method of T-nTP and DSA of a BCP. Moreover, on the basis of the combined process, we present the successful creation of an ultrahigh-density crossbar NiO_x/Pt memristive array on a flexible and transparent substrate that shows excellent unipolar resistive switching behavior.

RESULTS AND DISCUSSION

Replication of nanopatterns at the 8-inch wafer scale

The procedure of the T-nTP method to generate well-ordered nanopatterns with functionality on the 8-inch wafer level is schematically shown in fig. S1. It consists of two sequential steps of pattern replication (step 1) and transfer printing of the functional structure (step 2). In step 1, surface-patterned polymer replica films are produced by peeling off the spin-coated polymeric material from the Si master mold using an adhesive polyimide (PI) film. During the replication process, uniform surface contact and pressure between the PI film and polymer film is of paramount importance for successful large-area patterning. In step 2, the functional materials are initially formed on the surface of the replicated polymer pattern by physical vapor deposition (PVD). The functional nanostructure on the replica pattern is then transfer-printed on the 8-inch wafer via a short (≤20 s) contact and release process using a heat-rolling press system capable of supplying uniform pressure and heat. Appropriately applied heat weakens the adhesion between the adhesive film and the polymeric replica pattern, allowing the functional nanostructures on the polymer replica pattern to be transfer-printed on the substrates. Functional nanopatterns on the substrate are ultimately obtained after removing with solvent the residual polymer replica film used as a medium for the pattern transfer process.

Figure 1 shows the replication results of surface nanopatterns on an 8-inch wafer. The pattern geometry (e.g., aspect ratio) of the mold affects the yield of T-nTP during both polymer replication and pattern transfer printing. First, we prepared an 8-inch Si wafer consisting of approximately 50 chips with three line/space structures with different widths of 250 nm/250 nm, 500 nm/500 nm, and 1 μm/1 μm, fabricated by a conventional photolithography process, as shown in Fig. 1 (B and C) and fig. S2. The depths of the line patterns are identical in all cases at 250 nm, showing the well-defined structures with relatively low aspect ratios. Before the replication process, the 8-inch Si master mold was surface-treated with a hydroxyl-terminated polydimethylsiloxane brush to impart hydrophobicity

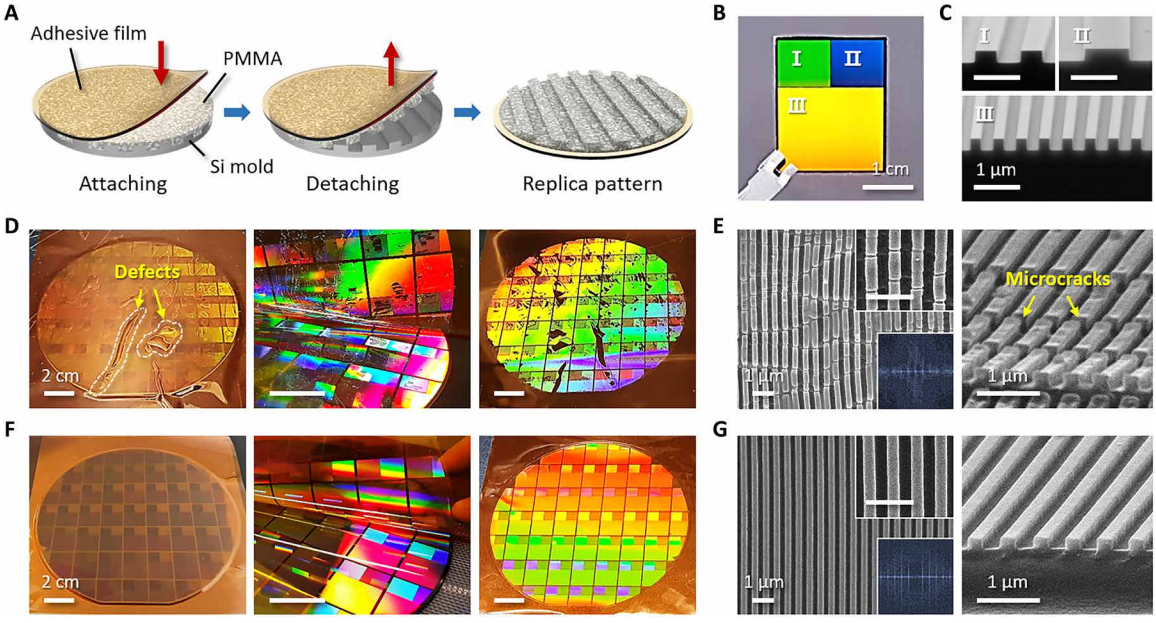

Fig. 1. Replication of nanopatterns at the 8-inch wafer. (**A**) Schematic illustration of the fabrication process of the polymer replica pattern. The spin-coated poly(methyl methacrylate) (PMMA) thin film on the Si master mold, consisting of nearly 50 chips, is peeled off using an adhesive PI film. (**B**) One chip with three types of line/space patterns makes up a Si wafer. The linewidths of the green area (top left), blue area (top right), and yellow area (bottom) are 500 nm/500 nm, 1 μm/1 μm, and 250 nm/250 nm, respectively. (**C**) Tilted scanning electron microscope (SEM) images of (B). All of the line patterns have the same depth of 250 nm. (**D**) Photograph images after attaching (left), during the detachment process (middle), and after detaching (right) during the replication process step, all done by hand. (**E**) Top-view and tilt-view SEM images of (D), showing defective replica patterns with distortions and many microcracks. (**F**) Photographs taken after attaching (left), during detachment step (middle), and after detaching (right) during the replication process step using a roll-pressing system. (**G**) Top-view and tilt-view SEM images of (F), showing well-defined PMMA line/space patterns. Scale bars, 1 cm (B), 1 μm [C, E, and G; insets in (E) and (G)], and 2 cm (D and F). Photo credit: T. W. Park (KICET and Korea University).

onto the Si surface for easy separation of the replica material from the master mold. After spin-coating poly(methyl methacrylate) (PMMA) dissolved in a mixture of toluene and acetone onto the hydrophobic surface of the Si mold, the spin-coated PMMA thin film was attached with an adhesive PI film, and the two films were subsequently detached together. When manually attaching and detaching the PI film, a defect-punctured PMMA replica pattern was obtained owing to the uneven contact between the PI film and the PMMA film through nonuniform pressure, resulting in many void defects and an abnormal line pattern with numerous microcracks, as shown in Fig. 1 (D and E). On the other hand, when using a laminating or rolling press system, replication of the PMMA surface pattern on the 8-inch wafer was successful with uniform contact at an appropriate amount of pressure on the entire surface, showing excellent pattern formation of well-defined line structures (Fig. 1, F and G, and figs. S3 and S4). These results suggest that uniform contact and pressure are crucial for large-scale pattern replication, offering a practical replication strategy for patterning on a much larger scale.

Principle of T-nTP over a large area

To transfer the functional nanostructures on the PMMA replica pattern on a large area, both uniform pressure and heat conduction over the entire patterning area are required during the contact printing process, as schematically illustrated in Fig. 2A. Initially, the transfer printing process, in common with the pattern replication process, requires regular perfect pressure to prevent the creation of void defects and/or microcracks through reliable contact between the functional material formed on the PMMA replica pattern and the target substrate. At the same time, a heat-injection process is also needed to move the functional nanostructures with the replica pattern onto the target substrate by weakening the adhesion between the adhesive PI film and the replica thin film. In general, PMMA material tends to undergo thermal expansion upon heating, whereas porous PMMA shrinks during heat treatment, depending on the porosity of the polymer. When spin-casting the PMMA solution onto the master mold, the porous PMMA replica pattern can be formed at room temperature (RT) by the evaporation of the residual solvent in the PMMA thin film. The porosity of the PMMA

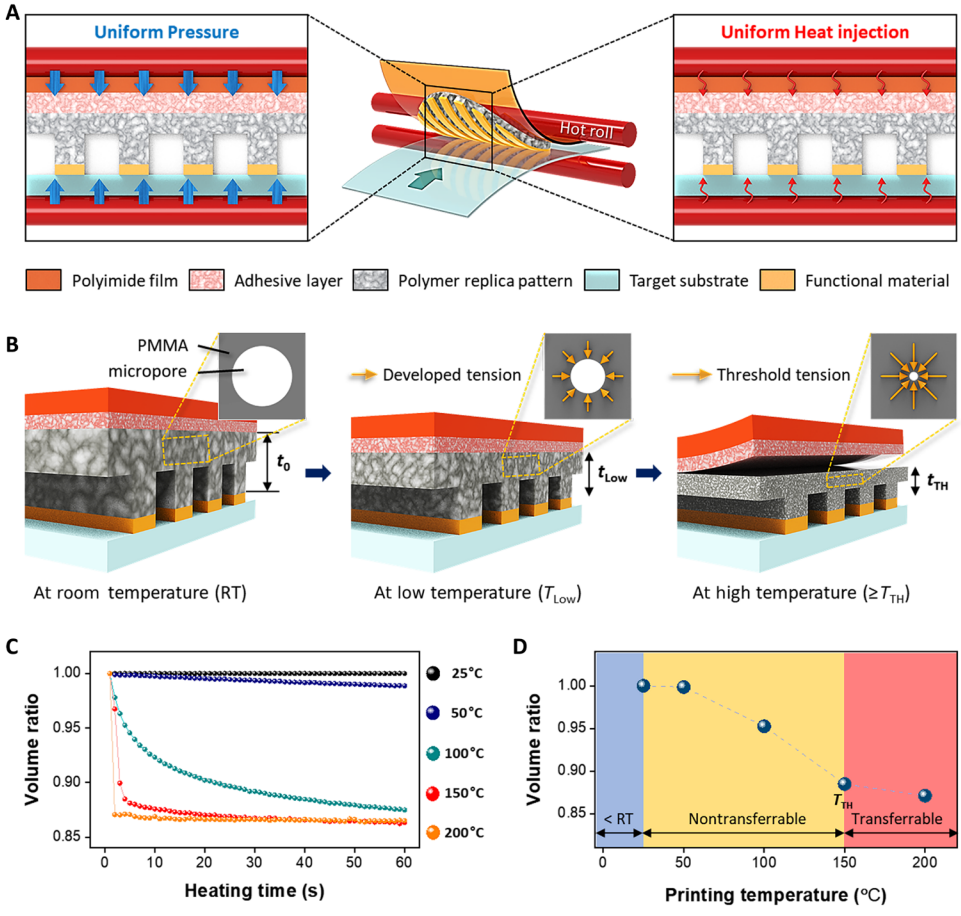

Fig. 2. Principle of T-nTP over a large area. (**A**) The concept of the T-nTP process using a heat-rolling press system that provides uniform pressure and heat. The functional nanostructure on the replicated polymer pattern can be transfer-printed onto the desired substrate by passing it between the heated rolls of the laminator. (**B**) Temperature dependency on the thickness of the PMMA film and transferability during the T-nTP process. The thickness of the PMMA layer decreases in proportion with the printing temperature due to the extinction of micropores in the PMMA film. At the threshold temperature (T_{TH}), the PMMA pattern with a functional structure can be transferred onto the target substrate by the tension generated by the shrinkage of the PMMA. (**C**) Volume ratio of the PMMA thickness at various temperatures from 25°C (room temperature) to 200°C. (**D**) Graph of the heating time of 3 s versus the printing temperature, which suggests that well-defined pattern formation over a large area can be achieved at the minimum required temperature (T_{TH} ~ 150°C).

layer decreases in proportion with the increase in the temperature (RT < T_{Low} < T_{TH}) through contraction by heat, resulting in thermal shrinkage (t_0 > t_{Low} > t_{TH}) of the PMMA thin film to reduce the surface energy, as shown in Fig. 2B and fig. S5 (A to C). During the shrinkage process, tension develops owing to the extinction of microvoids in the PMMA, enabling the transfer of the pattern to the substrate through the separation between the PMMA film and the PI adhesive film at the threshold temperature (T_{TH}).

Figure 2C and fig. S5D present the temperature dependency of the volume ratio (reduced thickness divided by the initial thickness) of the PMMA thin film, as measured by an in situ reflectometry system at various temperatures from 25°C (RT) to 200°C. Figure 2D shows the volume ratios for various transfer printing temperatures at a heating time of 3 s, indicating the range of printing temperatures. The volume ratio at 150°C (T_{TH}) was notably decreased by approximately 0.88 at a heating time of 3 s, marking a shrinkage ratio of 12% and showing rapid saturation of the volume ratio. Considering the thermal expansion coefficient (7×10^{-5} to 7.7×10^{-5}) of PMMA (*37*), the effect of thermal expansion can be calculated to be 0.87 to 0.96% of the volume for heating to 150°C, which is overwhelmed by the volume shrinkage effect (>12%).

Even after stopping the heat treatment at 150°C (and subsequent cooling to RT), the reduced thickness of the PMMA film did not recover to the initial thickness. Also, reheating to 150°C, as shown in fig. S5D, did not restore the original thickness. The densification of PMMA by the thermal treatment was confirmed by a spectroscopic ellipsometry analysis, showing the increase of the refractive index by the thermal annealing (fig. S5C). These phenomena support the irreversible thermal shrinkage of the porous PMMA thin film by the heat treatment. Figure S6 displays the temperature dependency of the size and number of pores formed on the PMMA surface, evidently showing the increase of pore size approximately from 40 to100 nm by the heat treatment at 150°C. The existence of small pores, which induces thermal shrinkage, can be attributed to the residual solvents in the spun-cast PMMA film (*38*) followed by the evaporation of residual solvent. Combined characterization results such as changes of the film thickness and refractive index upon the thermal treatment, in situ monitoring of volume ratio, and observation of pores on the surface strongly support the idea that the spin-coated PMMA thin film is thermally contracted by densification through the extinction of pores in the PMMA thin film.

Pattern formation of various structures via the T-nTP process at the 8-inch wafer scale

To confirm the printable temperature range, we initially conducted the patterning process via the T-nTP method at the typical chip scale (2.2 cm by 1.8 cm), as shown in fig. S7. While the transfer yield showed a very low percentage below 150°C, the well-ordered Pt line structures on the PMMA replica pattern were completely transfer-printed without any loss of the transfer yield at 150°C. We also conducted a peel strength test at an angle of separation of 90° to measure the adhesion between the adhesive PI film and the PMMA replica film at various printing temperatures, as shown in Fig. 3B. As the temperature was increased from 25 to 150°C, the peeling strength decreased from approximately 152 to 36 N/m, a result that is inversely proportional to the transfer yield. These results clearly demonstrate that the transfer yield is highly dependent on the printing temperature, in very good agreement with the volume ratio measurement of the PMMA thin film mentioned above. During the transfer printing process at T_{TH}, the effects on other processing variables, such as the pressure and film thickness of the PMMA, should also be studied in future work.

On the basis of the results for the T-nTP method, to produce well-ordered patterns on an 8-inch wafer effectively, we used a simple and useful heat-rolling press system capable of providing both uniform pressure and heat (see movie S1: T-nTP process). The target substrates with low surface roughness and good thermal stability were chosen in view of the printing temperature of 150°C. Figure 3 shows the remarkable results of the pattern formation via the T-nTP process on the 8-inch wafer when using the heat-rolling press equipment. After Pt deposition on the 8-inch PMMA replica pattern by the PVD sputtering system, we transfer-printed Pt nanowires onto a transparent and flexible polyethylene terephthalate (PET) substrate for 25 s by passing them between two 150°C hot rolls, resulting in a completely printed 8-inch wafer pattern, as shown in Fig. 3C. The pattern quality of the printed Pt lines with a width of 250 nm at the center of the 8-inch wafer was analyzed by grazing-incidence small-angle x-ray scattering measurements, clearly indicating excellent pattern uniformity (fig. S8). We also demonstrate successful pattern transfer of Pt line structures on a rigid 8-inch Si wafer, showing periodically well-printed Pt line patterns with three linewidths, as shown in fig. S9. Meanwhile, when using the S-nTP method, the generation of a high-quality pattern cannot be achieved at the 8-inch wafer level despite the use of the rolling press system, as the solvent vapor cannot be fundamentally injected uniformly into the entire 8-inch area due to the evaporative nature of the solvent (fig. S10). Here, it should be emphasized that high-quality patterns on most 8-inch wafer materials with thermal endurance can be obtained for a short printing time of 25 s when reliably providing both uniform pressure and heat transfer at 150°C.

Figure 3 (D and E) indicates that the T-nTP process is highly applicable for the generation of patterns of various shapes and with various materials. First, specifically designed characters or images composed of nanopatterns can be obtained by selective printing using a shadow mask, as shown in Fig. 3D. Pt was partially sputter-deposited onto the PMMA replica pattern using an alphabetic shadow mask followed by transfer printing onto a flexible colorless PI substrate via T-nTP. A selectively printed VVIP pattern consisting of Pt line structures was successfully obtained by the shadowing T-nTP process, with this approach applicable to various objects to offer aesthetic sensibility. The periodic Pt line patterns can also be obtained on slippery surfaces (e.g., slide glass substrate) by T-nTP (fig. S11). Figure 3E shows several unusual pattern geometries for various semiconducting (NiO, WO_3, and GST) and metallic (Pt, Ag, and Pd) materials created by T-nTP using master molds of various and complex shapes. Diverse nanostructures, including a wave, a square, a nut, a zigzag, and an ellipse, were obtained by the T-nTP process, showing excellent pattern uniformity, as depicted in the unique fast Fourier transform patterns. These results indicate that the creation of specific patterns of other imaginable or designable structures can be realized by the versatile T-nTP method regardless of the pattern shape or material used.

High-density memristive NiO_x/Pt crossbar array via the T-nTP process

We now demonstrate how to obtain ultrahigh-resolution patterns of sub–20-nm lines and hierarchically 3D stacked nanostructures for high-density resistive memory applications using a combination

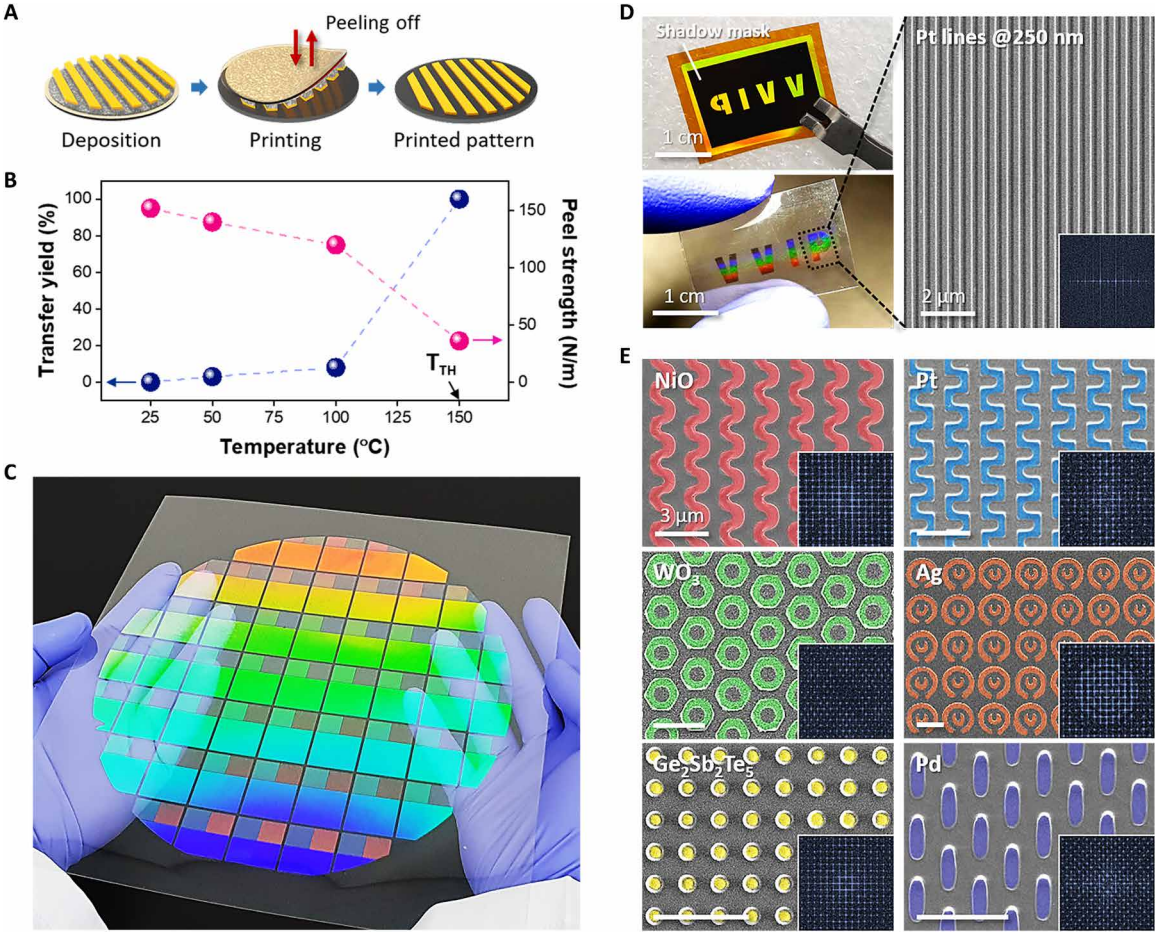

Fig. 3. Various pattern formation outcomes via the T-nTP process at the 8-inch wafer scale. (**A**) Procedure for the transfer printing of a functional nanopattern by T-nTP. (**B**) Temperature dependency on the transfer yield and peel strength between the adhesive layer and the PMMA replica pattern. The T_{TH} for perfect pattern transfer is 150°C. As the temperature was increased from 25 to 150°C, the peel strength decreased from 152 to 36 N/m, showing excellent pattern formation of functional materials. (**C**) Transfer-printed pattern on the 8-inch wafer on a transparent and flexible PET substrate by T-nTP. (**D**) Photographs and SEM images of transfer-printed letters of "V," "V," "I," and "P" consisting of 250-nm Pt lines on colorless PI film by a shadowing deposition process. (**E**) Colorized SEM images of the diverse pattern geometries created with various semiconducting (NiO, WO_3, and GST) and metallic (Pt, Ag, and Pd) materials via the T-nTP process. The inset images show fast Fourier transform patterns of the corresponding SEM images. Scale bars: 1 cm [top/left in (D), bottom/left in (D)], 2 μm [right in (D)], and 3 μm (E). Photo credit: T. W. Park (KICET and Korea University).

of the T-nTP method and DSA with a BCP. Initially, we used a cylinder-forming poly(styrene-*b*-dimethylsiloxane) (PS-*b*-PDMS) BCP to obtain an ultrafine SiO_x line-type template (fig. S12, A and B) (*39*). A highly ordered Pt nanowire pattern with a width of 14 nm was then obtained using a self-assembled 18-nm SiO_x line pattern via DSA of the PS-*b*-PDMS BCP as a master mold, as shown in Fig. 4A. Figure 4B displays the well-defined crossbar 3D Pt nanoscaffolds created by a twice-repeated sequential T-nTP process with 0° and 90° angles. The printing angles or alignment of the 3D stacked structure were manually controlled using a protractor. On the basis of the combined T-nTP process with DSA, we exhibit the creation of an ultrahigh-density crossbar NiO_x/Pt memristive array on a flexible and transparent PET substrate. Figure 4C presents a schematic diagram of the electrical measurement of the crossbar NiO_x/Pt resistive memory device on the flexible substrate, showing its expected unipolar resistive switching mechanism through the formation of conductive Ni filaments within the NiO_x nanowire when an appropriate set voltage is applied. Figure 4D and fig. S12C show the nanotransfer-printed crossbar NiO_x/Pt resistive memory device fabricated by the double sequential T-nTP process. To confirm the successful formation of the crossbar NiO_x/Pt nanostructure, we observed the structure by SEM, transmission electron microscopy (TEM), energy-dispersive spectrometry (EDS), and electron energy-loss spectroscopy (EELS). The elemental EDS mapping images for Pt and Ni and the EELS data clearly present the well-defined NiO_x/Pt structure, for which the images were obtained from the measurements with top-view and cross-sectional scanning TEM data (*40*).

At this point, we present the memory characteristics of the crossbar NiO_x/Pt nanodevice. To measure the resistive switching behaviors of the ultrafine NiO_x/Pt memristors, conductive AFM (C-AFM) was used. As a top electrode, a Pt-coated AFM tip with a radius of 30 nm was used due to the small device size. While the bottom electrode of Pt was grounded, a bias voltage was swept over the NiO_x arrays from 0 to 10 V with a step size of 0.2 V using the Pt AFM tip to investigate the current (*I*)–voltage (*V*) characteristics. The compliance current (I_{cc}) was set to 20 μA to protect the samples.

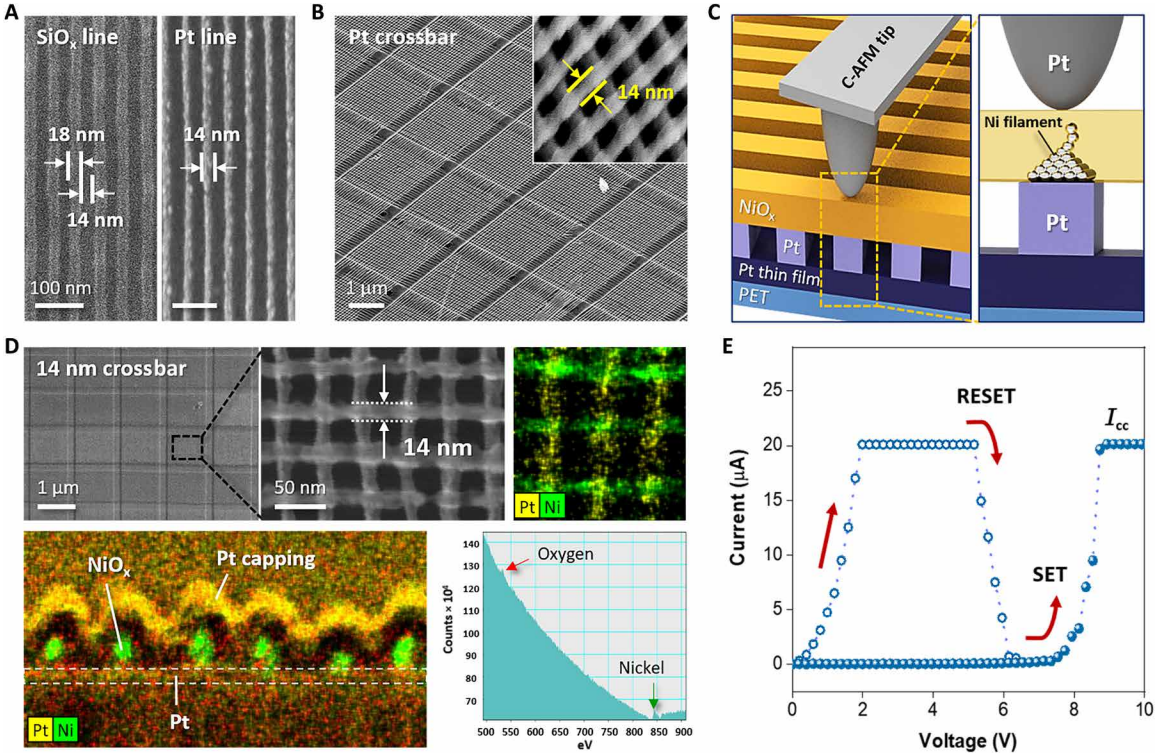

Fig. 4. High-density memristive crossbar NiO_x/Pt nanoarrays via the T-nTP process on a flexible and transparent PET substrate. (**A**) (Left) Self-assembled SiO_x line with an 18-nm-width master template formed by the DSA of a cylinder-forming PS-*b*-PDMS BCP and (right) the transferred 14-nm-width Pt line pattern via the T-nTP process using the SiO_x line master mold. (**B**) Three-dimensional hierarchical ultrahigh-resolution Pt crossbar structure produced by a repeated T-nTP process with different angles (0° and 90°). (**C**) Schematic illustration of the resistive memory device structure and its resistive switching mechanism through the formation of a Ni filament within NiO_x nanowire. (**D**) High-density NiO_x/Pt crossbar resistive memory device created by the T-nTP process. (Top left and top middle) Top-view SEM images, (top right) top-view transmission electron microscopy (TEM)–energy-dispersive spectrometry (EDS) elemental mapping image, (bottom left) cross-sectional TEM-EDS image, and (bottom right) an electron energy-loss spectroscopy measurement result for the NiO_x line structure. (**E**) *I-V* curve of the NiO_x/Pt memristive structure. Scale bars: 100 nm (A), 1 μm [(B) and top left in (D)], and 50 nm [top center in (D)].

The NiO_x/Pt nanoscale memristors clearly showed conventional unipolar switching behavior, as shown in Fig. 4E. The reset current, at which the low-resistance state changes to a high-resistance state, was measured to be 20 μA, while the measured set and reset voltages were around 7.4 and 5.2 V, respectively. These results indicate that simple and useful nanofabrication of many other nonvolatile memory devices can be realized if the approach of T-nTP combined with the BCP process is applied to other systems for various functional materials and structures.

CONCLUSION

In summary, we demonstrated a very useful T-nTP process that effectively generates well-ordered nanostructures over a large area by using a heat-rolling press system capable of providing both uniform pressure and heat. We successfully realized various complex nanopatterns on the 8-inch wafer, such as wave, square, nut, zigzag, and elliptical structures, composed of a variety of metallic and semiconducting materials with functionalities on diverse substrates through a uniform heat-injection process via solvent-free T-nTP. Furthermore, we realized the formation of patterns of ultrafine (≤20 nm) hierarchical 3D nanostructures using a method that combines T-nTP and the DSA of a BCP. We also systemically demonstrated how to obtain a high-density crossbar NiONiO_x/Pt memristive nanoarray on a transparent and flexible PET substrate, showing excellent unipolar resistive switching behavior. We expect that the proposed state-of-the-art T-nTP process combined with other emerging patterning techniques will be especially useful for combined high-throughput nanofabrication of many other devices over much larger areas.

MATERIALS AND METHODS

Preparation of an 8-inch Si master mold

The 8-inch Si master mold consisting of three line/space widths (250 nm/250 nm, 500 nm/500 nm, and 1 μm/1 μm) with a depth of 250 nm was fabricated by conventional KrF photolithography and reactive ion etching (RIE). After spin-coating the positive photoresist (PR, Dongjin Semichem Co. Ltd.) with a thickness of 400 nm on the 8-inch Si wafer, the wafer was exposed using a KrF scanner (Nikon, NSR-S203B) and was then developed using a developer solution (tetramethylammonium hydroxide; Dongjin Semichem Co. Ltd.). The remaining PR patterns were used as an etch mask to pattern the Si with CF_4 plasma by means of RIE.

Fabrication of the sub–20-nm SiO_x line master mold

To obtain a well-ordered SiO_x line pattern, we used DSA of a Si-containing, cylinder-forming PS-*b*-PDMS BCP (SD45) with a

volume fraction of PDMS (f_{PDMS}) of 33.7% and a molecular weight (MW) of 45.5 kg/mol. After spin-coating the SD45 BCP dissolved in toluene on the topographically patterned template, the BCP thin film was annealed in a binary solvent of toluene and heptane at 65°C for 10 min. The sample was then etched by CF_4 plasma [gas flow rate, 30 standard cubic centimeters per minute (sccm); working pressure, 15 mtorr; plasma power, 60 W; etching time, 20 s] and O_2 plasma (gas flow rate, 30 sccm; working pressure, 15 mtorr; plasma power, 60 W; etching time, 30 s), finally resulting in a self-assembled, highly ordered sub–20-nm SiO_x line structure with a line/space width of 18 nm/14 nm.

Replication at the 8-inch wafer scale from the Si master pattern

Before the replication step, the patterned surface of the 8-inch Si master mold was treated with a PDMS (Polymer Source Inc.) brush at 130°C for the simple separation of the PMMA replica film from the master mold. After spin-coating the replica material PMMA with an MW of 100 kg/mol (Sigma-Aldrich) dissolved in a binary solvent of toluene and acetone, the replicated PMMA film was separated from the master mold by an adhesive PI film (3M Inc.), done using a laminator system that provided uniform pressure.

Pattern transfer printing by using a heat-rolling press system

To transfer functional patterns at a wafer scale, a heat-rolling press system (LAMIART-470 LSI, GMP Corp.) was used. The laminator system has four rolls encapsulated by elastic silicone rubber, which can provide both uniform heat and pressure by controlling the roll gap and temperature, respectively. While the rolling speed is controllable from 200 to 1500 mm/min, the printing speed on the 8-inch wafer was set as 500 mm/min.

Peel strength measurement

A peeling-off test was conducted using a tensile force test machine (FGJN-50, Nidec-Shimpo Corp.). After attaching the PI film onto the target substrate, the adhesive PI film was peeled off from the polymer replica pattern at 90°.

In situ thickness measurement of polymer thin films

The thicknesses of the initial and swollen PMMA thin films were measured using a reflectometer (F20-UV, Filmetrics Inc.) with a wavelength range of 350 to 1100 nm. The volume ratios of the thin films were calculated by dividing the measured thickness by the initial thickness.

Measurement of the RS operation of the resistive memory device

A resistive memory switching measurement was taken at RT using a C-AFM (MFP-3D-SA, Asylum Research) device with a Pt-coated C-AFM tip (EFM tips, NanoWorld). The resistive switching behavior of the NiO_x-Pt crossbar array was measured during operation in the range of 0 to 10 V after investigating the appropriate operating conditions, while the compliance current was set to 20 μA.

SUPPLEMENTARY MATERIALS

Supplementary material for this article is available at http://advances.sciencemag.org/cgi/content/full/6/31/eabb6462/DC1

REFERENCES AND NOTES

1. J.-H. Ahn, H.-S. Kim, K. J. Lee, S. Jeon, S. J. Kang, Y. Sun, R. G. Nuzzo, J. A. Rogers, Heterogeneous three-dimensional electronics by use of printed semiconductor nanomaterials. *Science* **314**, 1754–1757 (2006).
2. J.-P. Colinge, C.-W. Lee, A. Afzalian, N. D. Akhavan, R. Yan, I. Ferain, P. Razavi, B. O'neill, A. Blake, M. White, A.-M. Kelleher, B. McCarthy, R. Murphy, Nanowire transistors without junctions. *Nat. Nanotechnol.* **5**, 225–229 (2010).
3. S.-h. Shin, B. Hwang, Z.-J. Zhao, S. H. Jeon, J. Jung, J.-H. Lee, B.-K. Ju, J.-H. Jeong, Transparent displays utilizing nanopatterned quantum dot films. *Sci. Rep.* **8**, 2463 (2018).
4. A. Russo, B. Y. Ahn, J. J. Adams, E. B. Duoss, J. T. Bernhard, J. A. Lewis, Pen-on-paper flexible electronics. *Adv. Mater.* **23**, 3426–3430 (2011).
5. J. Kim, J. K. Koh, B. Kim, J. H. Kim, E. Kim, Nanopatterning of mesoporous inorganic oxide films for efficient light harvesting of dye-sensitized solar cells. *Ange. Chem. Inter. Ed.* **51**, 6864–6869 (2012).
6. J. Yoon, L. Li, A. V. Semichaevsky, J. H. Ryu, H. T. Johnson, R. G. Nuzzo, J. A. Rogers, Flexible concentrator photovoltaics based on microscale silicon solar cells embedded in luminescent waveguides. *Nat. Commun.* **2**, 343 (2011).
7. W. Seung, M. K. Gupta, K. Y. Lee, K.-S. Shin, J.-H. Lee, T. Y. Kim, S. Kim, J. Lin, J. H. Kim, S.-W. Kim, Nanopatterned textile-based wearable triboelectric nanogenerator. *ACS Nano* **9**, 3501–3509 (2015).
8. Y. Hu, L. Lin, Y. Zhang, Z. L. Wang, Replacing a battery by a nanogenerator with 20 V output. *Adv. Mater.* **24**, 110–114 (2012).
9. B. H. Mun, B. K. You, S. R. Yang, H. G. Yoo, J. M. Kim, W. I. Park, Y. Yin, M. Byun, Y. S. Jung, K. J. Lee, Flexible one diode-one phase change memory array enabled by block copolymer self-assembly. *ACS Nano* **9**, 4120–4128 (2015).
10. B. K. You, W. I. Park, J. M. Kim, K.-I. Park, H. K. Seo, J. Y. Lee, Y. S. Jung, K. J. Lee, Reliable control of filament formation in resistive memories by self-assembled nanoinsulators derived from a block copolymer. *ACS Nano* **8**, 9492–9502 (2014).
11. W. I. Park, J. M. Yoon, M. Park, J. Lee, S. K. Kim, J. W. Jeong, K. Kim, H. Y. Jeong, S. Jeon, K. S. No, J. Y. Lee, Y. S. Jeong, Self-assembly-induced formation of high-density silicon oxide memristor nanostructures on graphene and metal electrodes. *Nano Lett.* **12**, 1235–1240 (2012).
12. P. B. Catrysse, S. Fan, Nanopatterned metallic films for use as transparent conductive electrodes in optoelectronic devices. *Nano Lett.* **10**, 2944–2949 (2010).
13. M. Kim, D. Ha, T. Kim, Cracking-assisted photolithography for mixed-scale patterning and nanofluidic applications. *Nat. Commun.* **6**, 6247 (2015).
14. A. Turchanin, M. Schnietz, M. El-Desawy, H. H. Solak, C. David, A. Gölzhäuser, Fabrication of molecular nanotemplates in self-assembled monolayers by extreme-ultraviolet-induced chemical lithography. *Small* **3**, 2114–2119 (2007).
15. W. I. Park, K. Kim, H.-I. Jang, J. W. Jeong, J. M. Kim, J. Choi, J. H. Park, Y. S. Jung, Directed self-assembly with sub-100 degrees celsius processing temperature, sub-10 nanometer resolution, and sub-1 minute assembly time. *Small* **8**, 3762–3768 (2012).
16. W. I. Park, J. M. Kim, J. W. Jeong, Y. S. Jung, Deep-nanoscale pattern engineering by immersion-induced self-assembly. *ACS Nano* **8**, 10009–10018 (2014).
17. M. S. Onses, C. Song, L. Williamson, E. Sutanto, P. M. Ferreira, A. G. Alleyne, P. F. Nealey, H. Ahn, J. A. Rogers, Hierarchical patterns of three-dimensional block-copolymer films formed by electrohydrodynamic jet printing and self-assembly. *Nat. Nanotechnol.* **8**, 667–675 (2013).
18. S. O. Kim, H. H. Solak, M. P. Stoykovich, N. J. Ferrier, J. J. De Pablo, P. F. Nealey, Epitaxial self-assembly of block copolymers on lithographically defined nanopatterned substrates. *Nature* **424**, 411–414 (2003).
19. S. Park, C. Padeste, H. Schift, J. Gobrecht, T. Scharf, Chemical nanopatterns via nanoimprint lithography for simultaneous control over azimuthal and polar alignment of liquid crystals. *Adv. Mater.* **17**, 1398–1401 (2005).
20. D. Falconnet, D. Pasqui, S. Park, R. Eckert, H. Schift, J. Gobrecht, R. Barbucci, M. Textor, A novel approach to produce protein nanopatterns by combining nanoimprint lithography and molecular self-assembly. *Nano Lett.* **4**, 1909–1914 (2004).
21. M. K. Choi, J. Yang, K. Kang, D. C. Kim, C. Choi, C. Park, S. J. Kim, S. I. Chae, T.-H. Kim, J. H. Kim, T. Hyeon, D.-H. Kim, Wearable red–green–blue quantum dot light-emitting diode array using high-resolution intaglio transfer printing. *Nat. Commun.* **6**, 7149 (2015).
22. J. W. Jeong, W. I. Park, L.-M. Do, J.-H. Park, T.-H. Kim, G. Chae, Y. S. Jung, Nanotransfer printing with sub-10 nm resolution realized using directed self-assembly. *Adv. Mater.* **24**, 3526–3531 (2012).
23. J. K. Hwang, S. Cho, J. M. Dang, E. B. Kwak, K. Song, J. Moon, M. M. Sung, Direct nanoprinting by liquid-bridge-mediated nanotransfer moulding. *Nat. Nanotechnol.* **5**, 742–748 (2010).
24. D. M. Eigler, E. K. Schweizer, Positioning single atoms with a scanning tunnelling microscope. *Nature* **344**, 524–526 (1990).
25. S. W. Lee, B.-K. Oh, R. G. Sanedrin, K. Salaita, T. Fujigaya, C. A. Mirkin, Biologically active protein nanoarrays generated using parallel dip-pen nanolithography. *Adv. Mater.* **18**, 1133–1136 (2006).

26. K.-B. Lee, S.-J. Park, C. A. Mirkin, J. C. Smith, M. Mrksich, Protein nanoarrays generated by dip-pen nanolithography. *Science* **295**, 1702–1705 (2002).
27. J. Zaumseil, M. A. Meitl, J. W. P. Hsu, B. R. Acharya, K. W. Baldwin, Y.-L. Loo, J. A. Rogers, Three-dimensional and multilayer nanostructures formed by nanotransfer printing. *Nano Lett.* **3**, 1223–1227 (2003).
28. A. J. Baca, M. A. Meitl, H. C. Ko, S. Mack, H.-S. Kim, J. Dong, P. M. Ferreira, J. A. Rogers, Printable single-crystal silicon micro/nanoscale ribbons, platelets and bars generated from bulk wafers. *Adv. Funct. Mater.* **17**, 3051–3062 (2007).
29. B. Hwang, S.-H. Shin, S.-H. Hwang, J.-Y. Jung, J.-H. Choi, B.-K. Ju, J.-H. Jeong, Flexible plasmonic color filters fabricated via nanotransfer printing with nanoimprint-based planarization. *ACS Appl. Mater. Interfaces* **9**, 27351–27356 (2017).
30. Y. Qi, J. Kim, T. D. Nguyen, B. Lisko, P. K. Purohit, M. C. McAlpine, Enhanced piezoelectricity and stretchability in energy harvesting devices fabricated from buckled PZT ribbons. *Nano Lett.* **11**, 1331–1336 (2011).
31. M. A. Meitl, Z.-T. Zhu, V. Kumar, K. J. Lee, X. Feng, Y. Y. Huang, I. Adesida, R. G. Nuzzo, J. A. Rogers, Transfer printing by kinetic control of adhesion to an elastomeric stamp. *Nat. Mater.* **5**, 33–38 (2006).
32. H. Yi, M. Seong, K. Sun, I. Hwang, K. Lee, C. Cha, T.-i. Kim, H. E. Jeong, Wet-responsive, reconfigurable, and biocompatible hydrogel adhesive films for transfer printing of nanomembranes. *Adv. Funct. Mater.* **28**, 1706498 (2018).
33. D. S. Wie, Y. Zhang, M. K. Kim, B. Kim, S. Park, Y.-J. Kim, P. P. Irazoqui, X. Zheng, B. Xu, C. H. Lee, Wafer-recyclable, environment-friendly transfer printing for large-scale thin-film nanoelectronics. *Proc. Natl. Acad. Sci. U.S.A.* **115**, E7236–E7244 (2018).
34. L. Xu, S. R. Gutbrod, A. P. Bonifas, Y. Su, M. S. Sulkin, N. Lu, H.-J. Chung, K.-I. Jang, Z. Liu, M. Ying, C. Lu, R. C. Webb, J.-S. Kim, J. I. Laughner, H. Cheng, Y. Liu, A. Ameen, J.-W. Jeong, G.-T. Kim, Y. Huang, I. R. Efimov, J. A. Rogers, 3D multifunctional integumentary membranes for spatiotemporal cardiac measurements and stimulation across the entire epicardium. *Nat. Commun.* **5**, 3329 (2014).
35. W.-H. Yeo, Y.-S. Kim, J. Lee, A. Ameen, L. Shi, M. Li, S. Wang, R. Ma, S. H. Jin, Z. Kang, Y. Huang, J. A. Rogers, Multifunctional epidermal electronics printed directly onto the skin. *Adv. Mater.* **25**, 2773–2778 (2013).
36. J. W. Jeong, S. R. Yang, Y. H. Hur, S. W. Kim, K. M. Baek, S. Yim, H.-I. Jang, J. H. Park, S. Y. Lee, C.-O. Park, Y. S. Jeong, High-resolution nanotransfer printing applicable to diverse surfaces via interface-targeted adhesion switching. *Nat. Commun.* **5**, 5387 (2014).
37. H. Warlimont, W. Martienssen, *Springer Handbook of Materials Data* (Springer Nature, Schwitzerland, AG, ed. 2, 2018).
38. X. Zhang, K. G. Yager, S. Kang, N. J. Fredin, B. Akgun, S. Satija, J. F. Douglas, A. Karim, R. L. Jones, Solvent retention in thin spin-coated polystyrene and poly(methyl methacrylate) homopolymer films studied by neutron reflectometry. *Macromolecules* **43**, 1117–1123 (2010).
39. Y. S. Jung, C. A. Ross, Orientation-controlled self-assembled nanolithography using a polystyrene−polydimethylsiloxane block copolymer. *Nano Lett.* **7**, 2046–2050 (2007).
40. W. Grogger, F. Hofer, B. Kraus, I. Rom, W. Sitte, P. Warbichler, EFTEM and EELS analysis of a Pt/NiO interface. *Microchim. Acta* **133**, 125–129 (2000).

Acknowledgments

Funding: This research was supported by the Global Frontier Program through the Global Frontier Hybrid Interface Materials (GFHIM) and Basic Private Research Program of the National Research Foundation of Korea (NRF) funded by the Ministry of Science, ICT & Future Planning (no. 2013M3A6B1078874 and no. NRF-2017R1D1A1B03034490). **Author contributions:** T.W.P., Y.S.J., and W.I.P. conceived the ideas for this study. T.W.P. principally performed the experiments. K.H.K., J.-H.L., and M.B. provided useful insights on the research. S.H., M.B., H.J., J.W.L., G.R.L., and S.H.K. contributed to the C-AFM, TEM, and EDS analyses. J.H.P. and H.-I.J. prepared the various nanotemplates. T.W.P., Y.S.J., and W.I.P. mainly wrote the majority of the paper. All authors contributed to discussions and writing of the paper. **Competing interests:** The authors declare that they have no competing interests. **Data and materials availability:** All data needed to evaluate the conclusions in the paper are present in the paper and/or the Supplementary Materials. Additional data related to this paper may be requested from the authors.

Submitted 9 March 2020
Accepted 17 June 2020
Published 29 July 2020
10.1126/sciadv.abb6462

Citation: T. W. Park, M. Byun, H. Jung, G. R. Lee, J. H. Park, H.-I. Jang, J. W. Lee, S. H. Kwon, S. Hong, J.-H. Lee, Y. S. Jung, K. H. Kim, W. I. Park, Thermally assisted nanotransfer printing with sub–20-nm resolution and 8-inch wafer scalability. *Sci. Adv.* **6**, eabb6462 (2020).